Theor Chem Acc (2012) 131:1239
DOI 10.1007/s00214-012-1239-2

REGULAR ARTICLE

Structural, energetic and response electric properties of cyclic selenium clusters: an ab initio and density functional theory study

Andrea Alparone

Received: 29 March 2012 / Accepted: 18 May 2012 / Published online: 5 June 2012

Abstract The geometries, relative stabilities, binding energies, second-order difference of total energy (Δ^2E), vertical ionization energies (VIEs), vertical electron affinities (VEAs) and dipole polarizabilities of neutral Se_2 and cyclic Se_n ($n = 3$–12) clusters have been systematically investigated using conventional ab initio [HF, MP2, MP3, MP4, CCSD, CCSD(T)] and density functional theory (B3LYP, CAM-B3LYP) levels with the Dunning's correlation-consistent (cc-pVDZ, aug-cc-pVDZ, d-aug-cc-pVDZ and aug-cc-pVTZ) and Sadlej (POL and POL-DK) basis sets. For each cluster size, various structural isomers have been considered and optimized to search for the lowest-energy structure. The effects of the geometry, basis set and theoretical level on the calculated properties have been discussed. The relative stability of the clusters has been analyzed using binding energy per atom, Δ^2E and VIE–VEA gap. The computed binding energies and VIEs have been compared with the available observed data. The calculated properties show a strong dependence upon the size and geometry of the cluster. The even-numbered Se_n with $n = 6$ and 8 are predicted to be relatively stable clusters. The physico-chemical properties of selenium clusters have been compared to those of the sulphur homologues. On passing from sulphur to selenium clusters the binding energy per atom decreases, whereas the mean dipole polarizability per atom increases.

Keywords Selenium clusters · Structures · Energetics · Ionization energy · Electron affinity · Dipole polarizabilities

1 Introduction

In recent years, atomic clusters have attracted considerable attention, since they are promising materials for applications in nanoelectronics and catalysis [1–3]. Atomic clusters show peculiar size effects, exhibiting properties often much different from those of their atomic states and bulk [1]. Therefore, structural characterization of clusters turns out to be a fundamental aim in material science [1, 2].

Since the mid-90s, selenium clusters were studied for their interesting photo-induced phenomena [4] and potential applications in the fabrication of semiconductor devices and high-efficiency photoelectrochemical cells [5–7]. Selenium systems were investigated for the design of switching devices to optical fibers in non-linear optics and as memory media [8, 9]. Zeolite/selenium composite materials received great attention for the development of nanostructured semiconductors [10–13]. Selenium in the forms of chains and/or rings can be easily introduced into zeolite cavities. Their optical spectra can be studied in visible or near UV spectral regions, where zeolites are transparent [13]. In addition, there is also great interest in graphite intercalation systems with elemental selenium or selenium compounds as guests [14, 15].

Experimental information about small-sized selenium clusters is available from X-ray diffraction studies [16–18] and by Raman spectroscopy [19–22]. The structure of even-numbered Se_6, Se_8 and Se_{12} clusters introduced into mono-dimensional channels of $AlPO_4$-5 single crystals, mordenite and zeolite cavities were extensively characterized by

Electronic supplementary material The online version of this article (doi:10.1007/s00214-012-1239-2) contains supplementary material, which is available to authorized users.

A. Alparone (✉)
Department of Chemistry, University of Catania,
viale A. Doria 6, 95125 Catania, Italy
e-mail: agalparone@unict.it

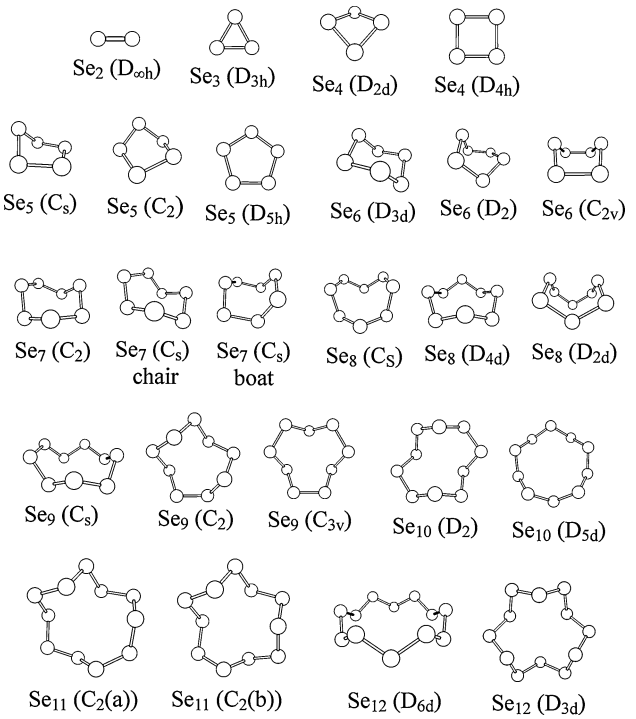

Fig. 1 Structure of neutral cyclic Se_n ($n = 2$–12) clusters

Raman spectroscopy [12, 13, 23–34]. Selenium clusters adsorbed into zeolite channels are bonded to each other and to the host matrices by van der Waals forces controlled by the polarizabilities of the clusters [21, 35]. On the theoretical side, geometries, relative stabilities, binding energies of selenium clusters are available from the literature [12, 36–49].

In this paper we studied theoretically the structure, relative stability, binding energy, ionization energy, electron affinity, static and dynamic electronic and vibrational polarizabilities of neutral Se_2 and cyclic Se_n ($n = 3$–12) clusters. The properties were computed in gas phase using conventional ab initio and density functional theory (DFT) methods. For each cluster size we considered a number of structural isomers. The investigated structures are shown in Fig. 1. The dependence of the stability and electronic properties on the cluster size was explored. We analyzed the performances of the employed basis sets and theoretical levels on the calculated properties. Despite numerous investigations about structural and spectroscopic properties of selenium clusters, experimental dipole polarizabilities are unknown to date, whereas theoretical estimates are available for Se_8 using the δ-function potential model of chemical bonding [50] and more recently for Se_2 using DFT computations [51].

The rest of the paper is organized as follows: the computational methods are described in the following section. The geometries, energetic properties, ionization energies, electron affinities and dipole polarizabilities are discussed in Sect. 3. Finally, our results are summarized in Sect. 4.

2 Computational details

The structures of neutral Se_2 and ring-like Se_n ($n = 3$–12) clusters were optimized in gas phase using the DFT-B3LYP functional [52, 53] with the Dunning's correlation-consistent cc-pVDZ basis set [54]. The B3LYP/cc-pVDZ geometries were then used in the subsequent calculations.

The electronic polarizability components α_{ij}^{e} ($i, j = x, y, z$) were determined as second-order derivatives of total energy (E) with respect to external electric fields (F):

$$E(F) = E(0) - \sum_i \mu_i F_i - \frac{1}{2}\sum_i \alpha_{ij}^{e} F_i F_j - \cdots \quad (1)$$

$$\alpha_{ij}^{e} = -\frac{\partial^2 E}{\partial F_i \partial F_j}|_{F=0} \quad (2)$$

The static electronic polarizabilities were evaluated analytically at the Hartree–Fock (HF) level through the Coupled-Perturbed HF theory (CP-HF) [55, 56]. At Møller–Plesset perturbation theory MPn ($n = 2, 3, 4$) and coupled-cluster (CC) theory accounting for singles and doubles (CCSD) and noniterative triple excitations [CCSD(T)], the α_{ij}^{e} values were computed numerically by means of a finite-field (FF) approach [57], using an F value of 0.005 a.u. The accuracy of the numerical procedure was checked by comparing the FF-HF and CP-HF α_{ij}^{e} values. Besides to the conventional ab initio methods, we used two common functionals such as the B3LYP and CAM-B3LYP [58]. As widely documented in the literature, the nature of the exchange-correlation DFT potential, especially its asymptotic behaviour, plays a crucial role in polarizability calculations. It is well-known that gradient-corrected functionals such as B3LYP generally overestimates the electronic polarizabilities [59], while recent reports have demonstrated that the long-range corrected CAM-B3LYP functional performs very well for the electronic polarizabilities [60–63]. The α_{ij}^{e} values were here calculated with the cc-pVDZ, augmented (aug-cc-pVDZ) and doubly-augmented (d-aug-cc-pVDZ) double-zeta, and triple-zeta (aug-cc-pVTZ) Dunning's correlation-consistent polarized valence basis sets. All these basis sets were retrieved from the EMSL basis set library [64, 65]. Additionally, we used the Sadlej's POL basis set, specifically built for polarizability computations [66]. All the above basis sets except the cc-pVDZ incorporate diffuse functions. The necessity of including diffuse functions in a basis set to accurately predict the electronic (hyper)polarizabilities has long been addressed [67].

Relativistic effects on the static electronic polarizabilities were evaluated for the smallest Se_n ($n = 2$–6) clusters within the scalar relativistic Douglas–Kroll (DK) approximation in the spin-averaged form [68–70]. For these computations we employed the B3LYP functional using the relativistic version of the Sadlej's POL basis set with contraction coefficients specifically generated within the DK approach (POL-DK) [71]. These calculations were carried out on geometries optimized at the B3LYP level with the relativistic cc-pVDZ-DK basis set [64, 65, 72].

Frequency-dependent electronic polarizabilities $\alpha_{ij}^{e}(-\omega;\omega)$ were calculated through the CP-HF method at the B3LYP/aug-cc-pVDZ level. Three characteristic laser wavelength (λ) values were considered: (1) Nd:YAG laser, $\lambda = 1{,}064$ nm ($\hbar\omega = 0.04282$ a.u.), (2) diode laser, $\lambda = 790$ nm ($\hbar\omega = 0.05767$ a.u.), (3) He/Ne laser, $\lambda = 633$ nm ($\hbar\omega = 0.07197$ a.u.).

For the lowest-energy isomers, we computed the vibrational contributions to the polarizability [73–76]. These calculations were carried out at the B3LYP/cc-pVDZ level on the geometry optimized at the same theoretical level. The vibrational polarizabilities are generally separated into pure vibrational (α^{pv}) and zero-point vibrational averaging (α^{ZPVA}) terms. The pure vibrational polarizability components α_{ij}^{pv} were determined under the double harmonic approximation as [73]:

$$\alpha_{ij}^{pv}(0;0) = [\mu^2]^{0,0} = \sum_{a}^{3N-6} \frac{\left(\frac{\partial \mu_i}{\partial Q_a}\right)_0 \left(\frac{\partial \mu_j}{\partial Q_a}\right)_0}{\omega_a^2} \tag{3}$$

where μ_i is the dipole moment component, Q_a is the normal mode coordinate and ω_a is the vibrational wavenumber value. The zero-point vibrational averaging (ZPVA) contributions were calculated as anharmonic electrical (n) and anharmonic mechanical (m) terms, $[\alpha]^{n,m}$ [77]:

$$\alpha^{ZPVA} = [\alpha]^{1,0} + [\alpha]^{0,1} \tag{4}$$

$$\text{with} \quad [\alpha]^{1,0} = \frac{1}{4}\sum_{a} \frac{\partial^2 \alpha^e}{\partial Q_a^2} \Big/ \omega_a \tag{5}$$

$$\text{and} \quad [\alpha]^{0,1} = -\frac{1}{4}\sum_{a} \left(\sum_{b} F_{abb}/\omega_b\right) \frac{\partial \alpha^e}{\partial Q_a} \Big/ \omega_a^2 \tag{6}$$

where F_{abb} is the cubic anharmonic force constant. In the present study the first derivatives were evaluated analytically, whereas the second derivatives were obtained by a finite differencing procedure using for each normal mode atomic displacements of ± 0.025 and ± 0.050 Å along the normal coordinate [78].

Polarizability is commonly expressed as a mean value ($\langle\alpha\rangle$) which is defined by

$$\langle\alpha\rangle = \frac{1}{3}(\alpha_{xx} + \alpha_{yy} + \alpha_{zz}) \tag{7}$$

We also reported the anisotropy of polarizability ($\Delta\alpha$) which is given by

$$\Delta\alpha = \left\{\frac{1}{2}\left[(\alpha_{xx} - \alpha_{yy})^2 + (\alpha_{xx} - \alpha_{zz})^2 + (\alpha_{yy} - \alpha_{zz})^2 + 6\left(\alpha_{xy}^2 + \alpha_{xz}^2 + \alpha_{yz}^2\right)\right]\right\}^{1/2} \tag{8}$$

In this work the polarizabilities were presented in atomic units (a.u.). The conversion factor from a.u. to S.I. is 1.648778×10^{-41} C^2 m^2 J^{-1}.

All calculations were performed with the Gaussian 09 package [79].

3 Results and discussion

3.1 Structures and energetics

For the neutral cyclic Se_n ($n = 4$–12) clusters we explored a number of low-lying isomers (Fig. 1), determining the most stable structure. The relative stabilities obtained at the B3LYP/aug-cc-pVDZ and HF/aug-cc-pVDZ levels are reported in Table 1. The structures optimized at the B3LYP/cc-pVDZ level are given in Figs. S1–S5 of the Supplementary Material. Vibrational analysis was performed at the B3LYP/cc-pVDZ level under the harmonic approximation, verifying if the lowest-energy isomer is an equilibrium structure on the potential energy surface (PES). The absence of imaginary vibrational wavenumbers is used to confirm that a structure is a stationary point on the PES.

The lowest-energy structure for the tetramer is the D_{2d} form, followed by the D_{4h} isomer, which is located 5–6 kcal/mol higher in energy. For the Se_5 and Se_7 clusters the C_s and C_2 cyclic forms are almost isoenergetic (being calculated to be within 1 kcal/mol), whereas for Se_6 our data indicate that the D_{3d} structure is largely favoured over the C_{2v} and D_2 isomers (by more than 10 kcal/mol). The lowest-energy structure for the octamer is the D_{4d} form. It is followed by the C_s and D_2 isomers which are located 8–9 and 18 kcal/mol above, respectively. The present B3LYP/aug-cc-pVDZ results for the Se_2–Se_8 series of clusters are consistent with those previously obtained by Kohara et al. [36] using the B3LYP/6-31G* level of calculation. For the largest Se_9, Se_{10}, Se_{11} and Se_{12} clusters the C_2, D_2, C_2 (form a) and D_{3d} structures are predicted to be the most stable isomers, respectively. A quite interesting case occurs for the Se_{10} clusters, for which at the B3LYP/aug-cc-pVDZ level the D_{5d} form lies only 0.25 kcal/mol above the D_2 form. Both the structures are true minima on the PESs [80], but the experimental geometry is not available so far.

The B3LYP/cc-pVDZ bond lengths and angles of the investigated Se_n ($n = 2$–12) isomers are given in Figs. S1–S5 of the Supplementary Material. Our structural

Table 1 Relative energies E_R (kcal/mol) of Se_n ($n = 4$–12) clusters

Cluster	Symm.	B3LYP	HF
Se_4	D_{2d}	0.00	0.00
	D_{4h}	5.61	4.95
Se_5	C_s	0.00	0.44
	C_2	0.36	0.00
	D_{5h}	33.24	27.11
Se_6	D_{3d}	0.00	0.00
	C_{2v}	10.44	14.52
	D_2	11.39	12.09
Se_7	C_s (chair)	0.00	0.97
	C_2	0.93	0.00
	C_s (boat)	4.34	9.40
Se_8	D_{4d}	0.00	0.00
	C_s	8.71	7.92
	D_{2d}	18.12	18.05
Se_9	C_2	0.00	0.00
	C_s	3.91	7.93
	C_{3v}	18.26	24.49
Se_{10}	D_2	0.00	0.00
	D_{5d}	0.25	7.10
Se_{11}	C_2 (a)	0.00	0.00
	C_2 (b)	2.12	0.79
Se_{12}	D_{3d}	0.00	0.00
	D_{6d}	16.18	21.27

Calculations were carried out with the aug-cc-pVDZ basis set on the B3LYP/cc-pVDZ geometry

parameters agree fairly well with those previously obtained for the Se_n ($n = 2$–4) clusters at the B3LYP/6-31G* and B3LYP/DZP++ levels [36, 49], for Se_5 at the B3LYP/6-311+G(d,p) and B3LYP/DZP++ levels [40, 49] and for Se_6 and Se_8 at the PBE0/cc-pVTZ and PBE0/6-311G(d) levels [41]. In addition, for the Se_2, Se_6 and Se_8 clusters, the present calculated gas-phase geometries are in reasonable agreement with the experimental ones determined in the solid (within 0.03–0.04 Å) [16–18]. It is of interest to explore the variation of the average Se–Se bond length ($\langle r \rangle$) for the Se_n clusters with the increase of the cluster size. The results for the lowest-energy isomer of each cluster are illustrated in Fig. 2. On passing from Se_2 to Se_4 the $\langle r \rangle$ value increases from 2.197 to 2.430 Å, then it reduces, converging to the asymptotic limit and showing a slight even-old alternation (even-numbered clusters having smaller $\langle r \rangle$ values). For both Se_{11} and Se_{12} the B3LYP/cc-pVDZ calculations predict an $\langle r \rangle$ value of 2.377 Å, which is 0.266 Å longer than the value for the S_{12} clusters obtained at the same level of calculation [81]. Finally, we note that the relativistic effects on the geometries of the Se_2–Se_6 clusters here estimated at the B3LYP/cc-pVDZ-DK level are almost negligible.

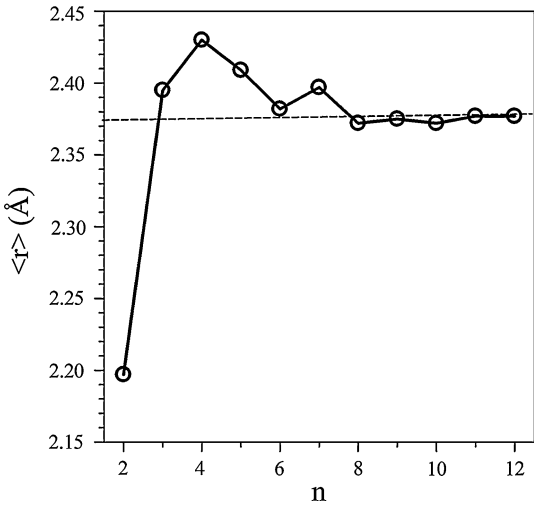

Fig. 2 Calculated average Se–Se bond length ($\langle r \rangle$) of cyclic Se_n ($n = 2$–12) clusters as a function of the cluster size. B3LYP/cc-pVDZ results

The relative stability of differently sized clusters can be evaluated by computing the binding energy per atom (BE/n) which is defined as follows:

$$\mathrm{BE}/n = [nE(\mathrm{Se}) - E(Se_n)]/n \quad (9)$$

where E(Se) is the energy of one selenium atom and $E(\mathrm{Se}_n)$ is the energy of a cluster with n selenium atoms. The calculated BE/n values for the lowest-energy isomer of each cluster are given in Table S1 of the Supplementary Material. The evolution of the BE/n data with the cluster size is represented in Fig. 3, which also includes the available experimental values taken from Ref. [82]. For all the employed theoretical methods, the BE/n value shows a slight even-old oscillation, rapidly converging to the asymptotic limit. On the whole, the BE/n value for Se_n with even n is greater than that for the neighbour clusters with odd n. As can be appreciated in Fig. 3, the HF/aug-cc-pVDZ calculations noticeably underestimate the observed and correlated BE/n data. The B3LYP/aug-cc-pVDZ BE/n values reproduce satisfactorily the experimental figures within 0.03–0.06 eV (1–3 %), whereas the MP2/aug-cc-pVDZ and CAM-B3LYP/aug-cc-pVDZ calculations give larger deviations (2–8 and 6–12 %, respectively). Additionally, our correlated BE/n data agree with previous DFT estimates calculated by Oligschleger et al. [47] and Pan et al. [48] for the Se_n ($n = 2$–8) clusters. In order to obtain an approximate estimate of BE/n in the limit for $n \to \infty$, we adopted the following extrapolation fitting expression [83, 84]:

$$\mathrm{BE}/n = a + b/n + c/n^2 \quad (10)$$

where a, b and c are least-squares fitting parameters. The asymptotic limit value nearly given by the a value is

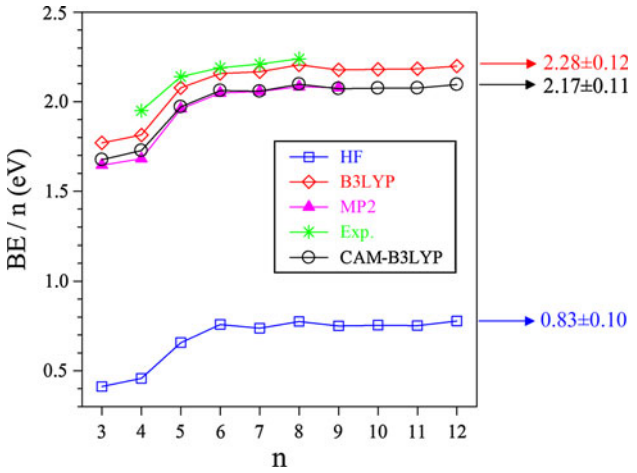

Fig. 3 Binding energy per atom (BE/n) of cyclic Se_n ($n = 3$–12) clusters as a function of the cluster size. Basis set: aug-cc-pVDZ

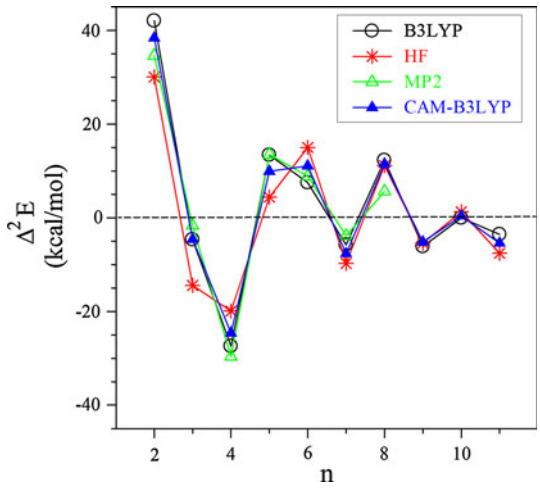

Fig. 4 Second-order difference of total energy (Δ^2E) of cyclic Se_n ($n = 2$–12) clusters as a function of the cluster size. Basis set: aug-cc-pVDZ

calculated to be 0.83 ± 0.10, 2.17 ± 0.11 and 2.28 ± 0.12 eV at the HF/aug-cc-pVDZ, CAM-B3LYP/aug-cc-pVDZ and B3LYP/aug-cc-pVDZ level, respectively. Interestingly, the B3LYP/aug-cc-pVDZ BE/n value for Se_n in the limit for $n \to \infty$ is estimated to be 0.44 eV smaller (-16 %) than that for the sulphur clusters, previously determined at the same level of calculation [81].

Besides to the BE/n property, the relative cluster stability can be evaluated calculating the second-order difference of total energy (Δ^2E) for the disproportionation reaction:

$$2Se_n \rightarrow Se_{n+1} + Se_{n-1}$$
$$\Delta^2E = E(Se_{n+1}) + E(Se_{n-1}) - 2E(Se_n) \quad (11)$$

This property is commonly recognized to represent the relative stability of a cluster of size n with respect to its neighbours with $n - 1$ and $n + 1$ atoms. A positive large Δ^2E value denotes an highly stable cluster. For the most stable isomer of each cluster the calculated Δ^2E values are collected in Table S2 of the Supplementary Material. Figure 4 shows the variation of the Δ^2E value with the cluster size. The plot shows odd–even alternation profiles. The even-numbered clusters except Se_4 generally exhibit greater Δ^2E values than their odd-numbered neighbours. This suggests that the even-numbered selenium clusters are relatively more stable than the neighbouring odd-numbered ones. Specifically, among the cyclic clusters, Se_6 and Se_8 display the highest positive Δ^2E values, in agreement with the data previously reported by Li et al. [44] for the Se_n ($n = 2$–7) clusters and with the S_n ($n = 2$–12) clusters [81]. Note that, the electron correlation effects on the Δ^2E values are noteworthy for the smallest clusters, whereas they are minimal for the largest ones (Se_n, $n \geq 6$).

3.2 Ionization energies and electron affinities

Vertical ionization energy (VIE) and electron affinity (VEA) were evaluated for the most stable isomer of each cluster size using the B3LYP level with the aug-cc-pVDZ basis set, through the usual ΔSCF scheme:

$$VIE = E_{cation} - E_{neutral} \quad (12)$$

$$VEA = E_{neutral} - E_{anion} \quad (13)$$

where $E_{neutral}$, E_{cation} and E_{anion} are the total energy for the neutral, cationic and anionic clusters, respectively, using the B3LYP/cc-pVDZ geometry of the neutral cluster. The total energy of the neutral ground state was computed using the restricted formalism (RB3LYP), whereas for the radical cation and anion states we employed the unrestricted UB3LYP function. It is important to mention that, for all cases the UB3LYP method gave only a negligible spin contamination ($S^2 \sim 0.75$).

The B3LYP/aug-cc-pVDZ VIEs and VEAs are collected in Table S3 of the Supplementary Material. The evolution of the calculated VIE values with the cluster size is plotted in Fig. 5, together with available experimental figures for comparison [85–87]. Theoretical VIEs were previously reported in the literature [44, 48, 88]. It is important to mention that, for some selenium clusters there is great uncertainty among the observed VIE values (up to 0.7 eV). Our VIE data are calculated to range from 7.65 eV (Se_{11}) to 9.22 eV (Se_2), in reasonable agreement with previous data for the Se_n ($n = 2$–8) clusters computed at the BLYP level [48]. For Se_6 and Se_8, the present VIE values agree very well (within 0.1 eV) with the most recent experimental data reported by Tribottet et al. [87]. In addition, as can be appreciated from the plot, for the clusters with $n \geq 4$ the calculated VIE values show an odd–even

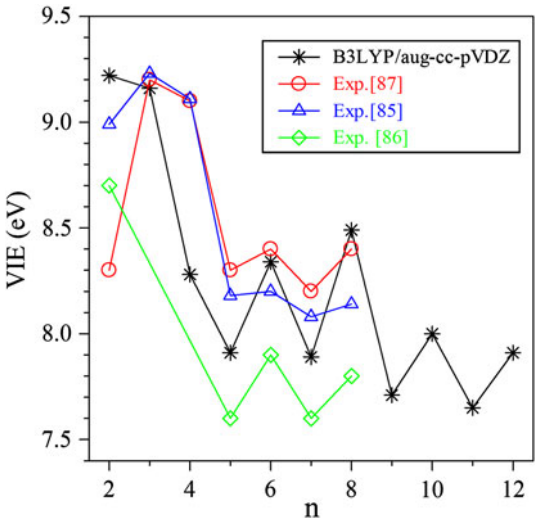

Fig. 5 Vertical ionization energy (VIE) of cyclic Se_n ($n = 2$–12) clusters as a function of the cluster size. B3LYP/aug-cc-pVDZ results

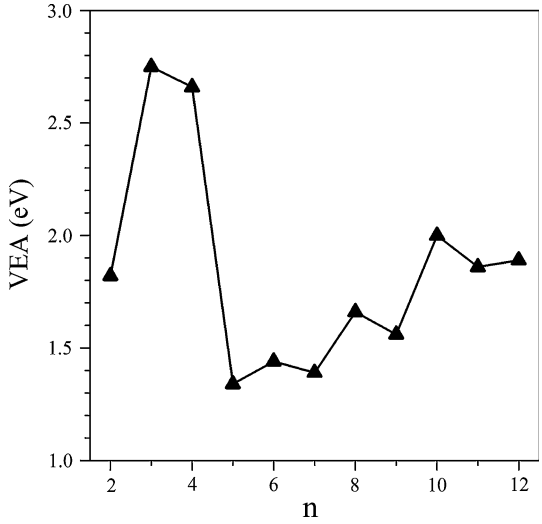

Fig. 6 Vertical electron affinity (VEA) of cyclic Se_n ($n = 2$–12) clusters as a function of the cluster size. B3LYP/aug-cc-pVDZ results

oscillation ($VIE_{even} > VIE_{odd}$), in agreement with the observed and calculated results.

In Fig. 6 we report the B3LYP/aug-cc-pVDZ VEA values as a function of the cluster size. To the best of our knowledge experimental adiabatic electron affinities (AEAs) values are available only for Se_2 (AEA = 1.94 ± 0.07 eV) and Se_3 (AEA > 2.2 eV) [89], while theoretical VEA and AEA estimates were previously obtained up to the Se_8 cluster using various DFT functionals [44, 49]. For all the investigated clusters the VEA values are positive (in the range 1.34–2.75 eV), implying that the anion is more stable than the parent neutral state. Present VEAs agree satisfactorily (within 0.06 eV) with those previously calculated at the B3LYP/DZP++ level for the Se_n ($n = 2$–5) clusters [49]. As for the VIEs, for the clusters with $n \geq 4$, the even-numbered clusters show larger VEA values compared to their immediate odd-numbered neighbours.

Using the B3LYP/aug-cc-pVDZ VIE and VEA data we determined the VIE–VEA gaps. The VIE–VEA gap furnishes an invaluable method in cluster stability analysis. Generally, a large gap corresponds to a high stability and chemical inertness. The VIE–VEA variation along the cluster size is depicted in Fig. 7. The range of the VIE–VEA values is calculated to be between 5.6 eV (Se_4) and 7.4 eV (Se_2). Local maxima are predicted for the even-numbered Se_6 and Se_8 clusters, in agreement with the behaviour of the calculated $\Delta^2 E$ values (Fig. 4). Note also that, the above results are in some consistency with the VIE–VEA profiles previously obtained on the sulphur series of clusters [81].

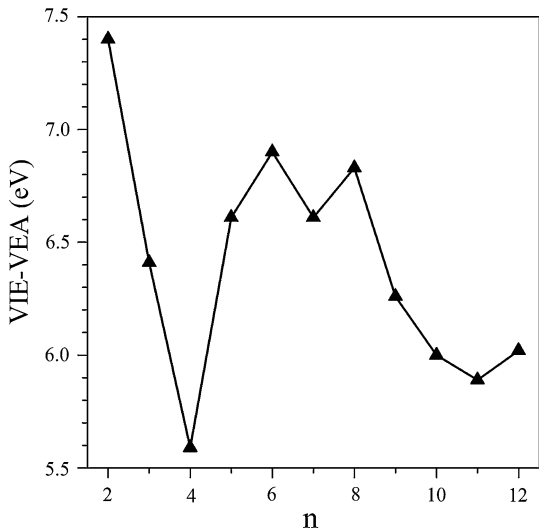

Fig. 7 VIE–VEA gap of cyclic Se_n ($n = 2$–12) clusters as a function of the cluster size. B3LYP/aug-cc-pVDZ results

3.3 Dipole polarizabilities

The dipole polarizability is one of the most important properties of clusters as it is closely related to their size, shape, stability and electronic structure [90]. Usually, experimental data correspond to the most stable isomers, therefore present discussion mainly will focus on the dipole polarizabilities of the lowest-energy clusters. However, other isomers will also be discussed briefly. To the best of our knowledge the experimental polarizabilities of selenium clusters are lacking so far. On the theoretical side, not much is known in the literature, some estimates are available for Se_8 [50] and more recently for Se_2 [51].

In Table 2 we compare the static electronic $\langle \alpha^e \rangle$ and $\Delta\alpha^e$ values for the smallest selenium clusters obtained using the conventional ab initio HF, MPn ($n = 2$, 3, 4), CCSD and CCSD(T) levels with the aug-cc-pVDZ basis set. Tables 3, 4 and 5 collect the static electronic $\langle \alpha^e \rangle$ and $\Delta\alpha^e$ values for

the selenium clusters calculated using the B3LYP and CAM-B3LYP functionals with a variety of Dunning's correlation-consistent basis sets (cc-pVDZ, aug-cc-pVDZ, d-aug-cc-pVDZ, aug-cc-pVTZ) as well as with the Sadlej's POL and POL-DK bases. The MP2/aug-cc-pVDZ, B3LYP/aug-cc-pVDZ and CAM-B3LYP/aug-cc-pVDZ methods nicely reproduce the CCSD(T)/aug-cc-pVDZ $\langle\alpha^e\rangle$ and $\Delta\alpha^e$ values within 1 and 5 %, respectively. The electron correlation effect on the $\langle\alpha^e\rangle$ value is negligible for the smallest cyclic Se_3 cluster, whereas it steadily increases as the size of the cluster increases. On the contrary, the electron correlation contribution to the $\Delta\alpha^e$ value decreases as the size of the selenium cluster increases. For the Se_n ($n = 2$–12) clusters, the CAM-B3LYP/aug-cc-pVDZ $\langle\alpha^e\rangle$ data are close to the B3LYP/aug-cc-pVDZ figures, with differences within 1–4 %.

In agreement with the usual literature data [81, 91, 92], the smallest cc-pVDZ basis set is inadequate to predict accurately the response electric properties, underestimating the polarizabilities obtained with diffuse basis sets. Specifically, with reference to the B3LYP functional, on passing from the cc-pVDZ to the aug-cc-pVDZ basis set the $\langle\alpha^e\rangle$ values for the series of the Se_2–Se_{12} clusters increase by 20–50 %. The further enlargement of the aug-cc-pVDZ basis set furnishes only marginal variations on the calculated polarizabilities. In facts, on going from the B3LYP/aug-cc-pVDZ to the B3LYP/d-aug-cc-pVDZ (B3LYP/aug-cc-pVTZ) level, the $\langle\alpha^e\rangle$ values increase by 1.0–3.8 % (1.5–4.0 %). In addition, we note that, for the Se_2–Se_6 clusters the B3LYP/aug-cc-pVTZ and B3LYP/POL polarizabilities are rather close to each other (see data in Tables 3, 4), the latter level underestimating the $\langle\alpha^e\rangle$ values of the former by 0.4–0.6 %. However it is important to notice that, the augmentation of the basis set reduces as the cluster size increases, in agreement with the results previously obtained on large-sized π-conjugative systems [93, 94]. The above results are in line with those previously obtained on the sulphur clusters using the Dunning's correlation-consistent basis sets [81].

Table 4 reports the comparison between the non-relativistic (B3LYP/POL) and relativistic (B3LYP/POL-DK) static electronic polarizabilities. The results for the Se_n ($n = 2$–6) clusters show that, the relativistic effects are somewhat negligible, increasing the non-relativistic $\langle\alpha^e\rangle$ values by only 0.1–0.5 %.

Interestingly, our B3LYP/aug-cc-pVTZ $\langle\alpha^e\rangle$ value of Se_2 correctly reproduces (within 0.2 a.u.) the datum previously reported by Torrent-Sucarrat et al. [51] using the same level of calculation. In addition, the $\langle\alpha^e\rangle$ value for Se_8 of 234.23 a.u. estimated by Lippincott et al. [50] through the δ-function potential model of chemical bonding is in satisfactory agreement with our datum of the D_{4d} structure computed at the HF/aug-cc-pVDZ level. The comparison

Table 2 Ab initio static electronic mean dipole polarizability $\langle\alpha^e\rangle$ (a.u.) and polarizability anisotropy $\Delta\alpha^e$ (a.u.) of Se_n ($n = 1$–6) clusters

Cluster	Symm.	HF		MP2		MP3		MP4-DQ		MP4-SDQ		MP4-SDTQ		CCSD		CCSD(T)	
		$\langle\alpha^e\rangle$	$\Delta\alpha^e$	$\langle\alpha^e\rangle$	$\Delta\alpha^e$	$\langle\alpha^e\rangle$	$\Delta\alpha^e$	$\langle\alpha^e\rangle$	$\Delta\alpha^e$	$\langle\alpha^e\rangle$	$\Delta\alpha^e$	$\langle\alpha^e\rangle$	$\Delta\alpha^e$	$\langle\alpha^e\rangle$	$\Delta\alpha^e$	$\langle\alpha^e\rangle$	$\Delta\alpha^e$
Se		23.73	4.70	23.91	5.36	24.01	5.60	24.05	5.65	24.05	5.64	24.11	5.68	24.09	5.70	24.18	5.80
Se_2	$D_{\infty h}$	60.68	59.92	50.63	30.25	52.43	35.42	53.22	37.49	54.55	41.20	53.68	38.31	56.32	46.00	55.91	44.37
Se_3	D_{3h}	79.12	32.44	78.87	27.39	78.52	27.97	78.74	28.16	79.01	28.17	79.27	27.56	78.99	28.01	79.22	27.49
Se_4	D_{2d}	107.17	42.80	107.57	38.34	106.69	38.45	106.91	38.70	107.39	38.90	107.99	38.51	107.45	38.94	108.00	38.70
Se_5	C_s	135.26	57.26	139.80	58.04												
Se_6	D_{3d}	164.91	71.39	169.50	71.93												

Calculations are carried out with the aug-cc-pVDZ basis set on the B3LYP/cc-pVDZ geometries

Table 3 Static electronic mean dipole polarizability $\langle \alpha^e \rangle$ (a.u.) of Se_n ($n = 1$–12) clusters

Basis set	Cluster	Symm.	$\langle \alpha^e \rangle$	Cluster	Symm.	$\langle \alpha^e \rangle$	Cluster	Symm.	$\langle \alpha^e \rangle$	Cluster	Symm.	$\langle \alpha^e \rangle$	Cluster	Symm.	$\langle \alpha^e \rangle$
cc-pVDZ	Se		11.43	Se_5	C_2	110.55	Se_7	C_2	168.05	Se_9	C_s	241.17	Se_{12}	D_{3d}	321.36
aug-cc-pVDZ (aug-cc-pVDZ)			24.75 (24.23)			141.92			210.00			294.19			389.20 (374.42)
d-aug-cc-pVDZ			27.08												
aug-cc-pVTZ			26.74												
cc-pVDZ	Se_2	$D_{\infty h}$	37.76		D_{5h}	106.59		C_s (boat)	169.80		C_{3v}	242.65		D_{6d}	389.88
aug-cc-pVDZ (aug-cc-pVDZ)			55.16 (55.18)			138.78			210.34			295.81			461.89
d-aug-cc-pVDZ			57.26												
aug-cc-pVTZ			57.39												
cc-pVDZ	Se_3	D_{3h}	58.56	Se_6	D_{3d}	136.52	Se_8	D_{4d}	203.30	Se_{10}	D_2	260.68			
aug-cc-pVDZ (aug-cc-pVDZ)			79.34 (78.61)			172.09 (168.16)			250.50 (242.69)			318.80 (306.74)			
d-aug-cc-pVDZ			82.37			174.48			252.98						
aug-cc-pVTZ			82.27			174.70									
cc-pVDZ	Se_4	D_{2d}	82.73		C_{2v}	137.87		C_s	197.75		D_{5d}	287.37			
aug-cc-pVDZ (aug-cc-pVDZ)			108.45 (107.05)			173.50			244.20			346.75			
d-aug-cc-pVDZ			111.42												
aug-cc-pVTZ			111.45												
cc-pVDZ		D_{4h}	81.83		D_2	135.16		D_{2d}	195.14	Se_{11}	C_2 (a)	292.66			
aug-cc-pVDZ (aug-cc-pVDZ)			107.47			171.03			240.98			358.96 (344.61)			
d-aug-cc-pVDZ															
aug-cc-pVTZ															
cc-pVDZ	Se_5	C_s	111.02	Se_7	C_s (chair)	169.73	Se_9	C_2	226.33		C_2 (b)	291.03			
aug-cc-pVDZ (aug-cc-pVDZ)			142.34 (138.54)			211.57 (205.43)			278.08 (268.48)			353.65			
d-aug-cc-pVDZ			144.90			213.97									
aug-cc-pVTZ			144.94												

Calculations are carried at the B3LYP level on the B3LYP/cc-pVDZ geometry. Value in parentheses refers to CAM-B3LYP calculations

Table 4 Comparison between non-relativistic and relativistic Douglas–Kroll (DK) static electronic mean dipole polarizabilities (a.u.) of Se_n (n = 2–6) clusters

Cluster	Symm.	B3LYP/POL[a]	B3LYP/POL-DK[b]
Se_2	$D_{\infty h}$	57.02	57.09
Se_3	D_{3h}	81.94	81.99
Se_4	D_{2d}	110.79	111.25
Se_5	C_s	144.16	144.76
Se_6	D_{3d}	173.80	174.63

[a] Calculations were carried out on the B3LYP/cc-pVDZ geometry

[b] Calculations were carried out on the B3LYP/cc-pVDZ-DK geometry

between the present data and the corresponding figures of the series of the S_n (n = 2–12) clusters [81], shows that on passing from the sulphur to the selenium clusters the B3LYP/aug-cc-pVDZ static $\langle\alpha^e\rangle$ values increase by 15–111 a.u. (38–40 %). Interestingly, for Se_4 (D_{2d} form) we determined the static HF/d-aug-cc-pVDZ $\langle\alpha^e\rangle$ value of 109.37 a.u. This value may be compared to the datum for As_4, previously reported by Maroulis and co-workers [95] using a basis set of similar quality ([7s6p4d]). The results show that $\langle\alpha^e\rangle$ (As_4) = 119.10 a.u. is higher than $\langle\alpha^e\rangle$ (Se_4) by 9 %. In addition, for Se_2 the HF/d-aug-cc-pVDZ $\langle\alpha^e\rangle$ value of 62.38 a.u. is smaller than $\langle\alpha^e\rangle$ (As_2) = 64.95 a.u. obtained by Maroulis and Xenides [96] using a more larger basis set ([20s15p12d4f]). The above results for the dimer and tetramer of selenium and arsenic clusters are consistent with the atomic polarizabilities of selenium and arsenic, which were previously predicted to be 3.77 and 4.31 a.u., respectively [97].

It is of great interest to explore the role of the geometry on the polarizabilities of the investigated clusters. As can be appreciated from the data reported in Table 3, in several cases the effect of the structure is dramatic. The order of the calculated $\langle\alpha^e\rangle$ values is shown below (based on the B3LYP/aug-cc-pVDZ computations):

Se_4 $D_{4h} \sim D_{2d}$
Se_5 $C_s \sim C_2 > D_{5h}$
Se_6 $C_{2v} \sim D_{3d} \sim D_2$
Se_7 C_s(chair) $\sim$ C_s(boat) $\sim$ C_2
Se_8 $D_{4d} \sim C_s \sim D_{2d}$
Se_9 $C_{3v} \sim C_s > C_2$
Se_{10} $D_{5d} > D_2$
Se_{11} C_2(a) $\sim$ C_2(b)
Se_{12} $D_{6d} > D_{3d}$

The above results reveal that, with the notable exception of Se_6, Se_7 and Se_8 clusters, the geometries can significantly influence the polarizability of the cyclic selenium clusters. It is also worth to note that, the minimum polarizability principle, which establishes that any system tends towards a state of minimum polarizability [98, 99], seems to works adequately for the largest Se_n (n = 10–12) clusters. In addition, we compare the electronic polarizabilities of the cyclic selenium clusters with those of the open forms. The B3LYP/aug-cc-pVDZ//B3LYP/cc-pVDZ $\langle\alpha^e\rangle$ values for the open Se_3 (C_{2v} symmetry) and Se_4 (C_{2v} symmetry) clusters are computed to be 95.41 and 126.94 a.u., respectively, which are higher than the values obtained for the corresponding ring-like structures by ca. 20 %. These results are in agreement with those previously determined for the open and closed forms of O_3 [100], S_3 [81] and S_4 [81].

Besides to the structural effects, we explored the size dependence on the calculated electronic polarizabilities. The results are displayed in Fig. 8. Using a similar expression to that previously employed to extrapolate the binding energy per atom in the limit for $n \rightarrow \infty$ ($\langle\alpha^e\rangle/n = a + b/n + c/n^2$), the asymptotic limit for the $\langle\alpha^e\rangle$ value per atom (the parameter a) is predicted to be 31.7 ± 0.6, 37.5 ± 0.8 and 35.5 ± 0.7 at the B3LYP/cc-pVDZ, B3LYP/aug-cc-pVDZ and CAM-B3LYP/aug-cc-pVDZ level, respectively. Interestingly, for the Se_n clusters the B3LYP/aug-cc-pVDZ $\langle\alpha^e\rangle/n$ value for $n \rightarrow \infty$ is calculated to be 11.4 a.u. greater (+44 %) than that for the sulphur clusters determined at the same level of calculation [81]. It is worth to note that, at all the theoretical levels the differential mean polarizability per atom $\langle\alpha^e\rangle$ (Se_n)/n − $\langle\alpha^e\rangle$ (Se) is positive for all the clusters, in agreement with the results on As_4 [95] and S_n (n = 2–12) clusters [81]. This behavior was previously elucidated for sulphur clusters on the basis of the polarizability contributions from the lone pairs [81]. On the other hand, for silicon clusters negative $\langle\alpha^e\rangle$ (Si_n)/n − $\langle\alpha^e\rangle$ (Si) values were obtained, denoting strong bonding effects [101, 102]. Additionally, in agreement with previous calculations obtained using the theory of atoms in molecules [103, 104], we notice an excellent linear relationship between the calculated $\langle\alpha^e\rangle$ values and the cluster volumes here calculated using the Monte-Carlo integration procedure implemented in the Gaussian 09 program (Fig. 9).

Table 5 lists the static $\Delta\alpha^e$ values for the investigated Se_n (n = 1–12) clusters obtained using the B3LYP and CAM-B3LYP levels with the Dunning's correlation-consistent basis sets. Differently from the $\langle\alpha^e\rangle$ data, when passing from the cc-pVDZ to the aug-cc-pVDZ basis set, the $\Delta\alpha^e$ values for the Se_2–Se_6 clusters decrease, whereas they increase for the largest clusters. As expected, the further augmentation of the basis set (aug-cc-pVDZ → d-aug-cc-pVDZ, aug-cc-pVDZ → aug-cc-pVTZ), produces only minimal effects on the $\Delta\alpha^e$ values. Except for the smallest Se_n (n = 2–4) clusters, the CAM-B3LYP calculations underestimate the B3LYP $\Delta\alpha^e$ data.

Table 5 Static electronic anisotropy of polarizability $\Delta\alpha^e$ (a.u.) of Se_n ($n = 1$–12) clusters

Basis set	Cluster	Symm.	$\Delta\alpha^e$	Cluster	Symm.	$\Delta\alpha^e$	Cluster	Symm.	$\Delta\alpha^e$	Cluster	Symm.	$\Delta\alpha^e$	Cluster	Symm.	$\Delta\alpha^e$
cc-pVDZ	Se		0.23	Se_5	C_2	67.67	Se_7	C_2	81.43	Se_9	C_s	155.68	Se_{12}	D_{3d}	166.52
aug-cc-pVDZ (aug-cc-pVDZ)			5.72 (5.39)			62.51			85.99			166.03			176.80 (161.81)
d-aug-cc-pVDZ			6.34												
aug-cc-pVTZ			5.72												
cc-pVDZ	Se_2	$D_{\infty h}$	50.37		D_{5h}	87.97		C_s (boat)	38.10		C_{3v}	163.10		D_{6d}	304.05
aug-cc-pVDZ (aug-cc-pVDZ)			42.08 (43.93)			70.28			41.93			169.46			325.57
d-aug-cc-pVDZ			48.70												
aug-cc-pVTZ			41.48												
cc-pVDZ	Se_3	D_{3h}	42.36	Se_6	D_{3d}	77.41	Se_8	D_{4d}	127.12	Se_{10}	D_2	135.79			
aug-cc-pVDZ (aug-cc-pVDZ)			27.23 (28.53)			76.88 (73.61)			134.94 (126.45)			144.82 (132.96)			
d-aug-cc-pVDZ			27.63			76.27			134.00						
aug-cc-pVTZ			27.89			75.88									
cc-pVDZ	Se_4	D_{2d}	50.84		C_{2v}	74.88		C_s	102.18		D_{5d}	202.05			
aug-cc-pVDZ (aug-cc-pVDZ)			39.43 (39.81)			74.70			109.09			216.80			
d-aug-cc-pVDZ			39.78												
aug-cc-pVTZ			38.70												
cc-pVDZ		D_{4h}	64.01		D_2	66.28		D_{2d}	76.45	Se_{11}	C_2(a)	144.05			
aug-cc-pVDZ (aug-cc-pVDZ)			46.50			66.94			80.70			155.14 (140.72)			
d-aug-cc-pVDZ															
aug-cc-pVTZ															
cc-pVDZ	Se_5	C_s	67.64	Se_7	C_s (chair)	46.39	Se_9	C_2	102.71		C_2(b)	144.61			
aug-cc-pVDZ (aug-cc-pVDZ)			62.73 (59.40)			45.27 (43.07)			110.11 (101.17)			155.26			
d-aug-cc-pVDZ			62.61			45.05									
aug-cc-pVTZ			62.02												

Calculations are carried at the B3LYP level on the B3LYP/cc-pVDZ geometry. Value in parentheses refers to the CAM-B3LYP calculations

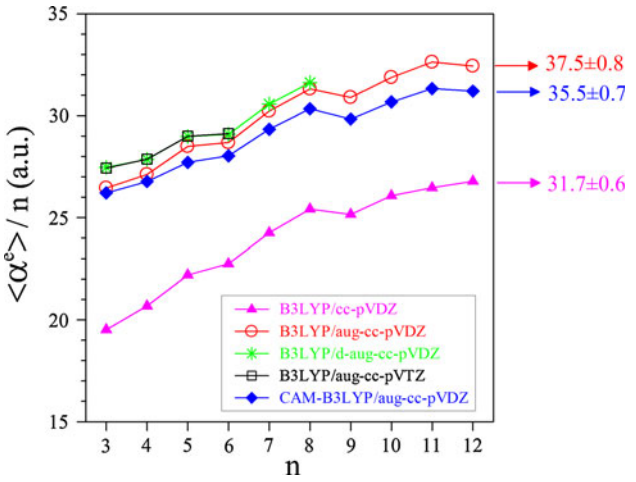

Fig. 8 Static electronic mean dipole polarizability per atom ($\langle\alpha^e\rangle/n$) of cyclic Se_n (n = 3–12) clusters as a function of the cluster size

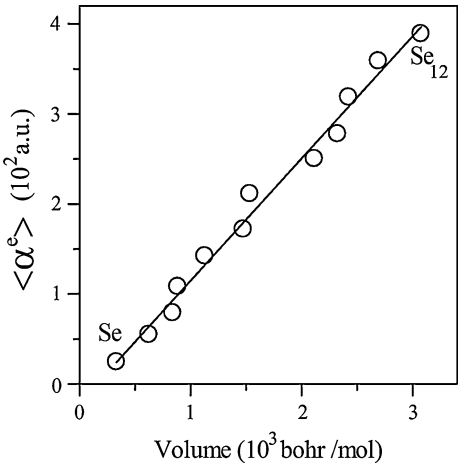

Fig. 9 Static electronic mean dipole polarizability of cyclic Se_n (n = 1–12) clusters as a function of the cluster volume. B3LYP/aug-cc-pVDZ results. $\langle\alpha^e\rangle = 1.36 \times$ Volume - 0.21 ($r^2 = 0.99$)

As for the calculated $\langle\alpha^e\rangle$ values, the $\Delta\alpha^e$ data for the Se_n isomers are strongly affected by the structure. The order of the computed $\Delta\alpha^e$ values for the studied clusters is reported below (based on the B3LYP/aug-cc-pVDZ calculations):

Se_4 $D_{4h} > D_{2d}$
Se_5 $D_{5h} > C_s \sim C_2$
Se_6 $D_{3d} \sim C_{2v} > D_2$
Se_7 C_s(chair) > C_2 > C_s(boat)
Se_8 $D_{4d} > C_s > D_{2d}$
Se_9 $C_{3v} \sim C_s > C_2$
Se_{10} $D_{5d} > D_2$
Se_{11} C_2(b) ~ C_2(a)
Se_{12} $D_{6d} > D_{3d}$

Table 6 Frequency-dependent electronic mean dipole polarizabilities (a.u.) of Se_n (n = 1–12) clusters

Cluster	Symm.	$\hbar\omega$ (a.u.)			
		0	0.04282	0.05767	0.07197
Se		24.75	25.04	25.29	25.75
Se_2	$D_{\infty h}$	55.16	56.39	57.54	60.02
Se_3	D_{3h}	79.34	80.63	81.84	85.10
Se_4	D_{2d}	108.45	110.04	111.48	114.38
Se_5	C_s	142.34	145.32	148.13	153.36
Se_6	D_{3d}	172.09	175.28	178.09	183.75
Se_7	C_s(a)	211.57	216.49	221.01	230.81
Se_8	D_{4d}	250.50	256.44	261.84	273.26
Se_9	C_2	278.08	285.21	291.93	307.60
Se_{10}	D_2	318.81	327.75	336.38	358.57
Se_{11}	C_2(a)	358.97	370.05	380.89	408.31
Se_{12}	D_{3d}	389.21	400.51	411.17	435.58

Calculations are carried at the B3LYP/aug-cc-pVDZ level on the B3LYP/cc-pVDZ geometry

Table 7 Mean pure vibrational α^{pv} (a.u.) and zero-point vibrational averaging α^{zpva} (a.u.) contributions to the static polarizability of Se_n (n = 2–12) clusters

Cluster	Symm.	α^{pv} $[\mu^2]^{0,0}$	α^{zpva}		
			$[\alpha]^{0,1}$	$[\alpha]^{1,0}$	$[\alpha]^{0,1} + [\alpha]^{1,0}$
Se_2	$D_{\infty h}$	0.00	0.005	0.00	0.05
Se_3	D_{3h}	0.07	0.12	0.01	0.13
Se_4	D_{2d}	0.10	0.13	0.02	0.15
Se_5	C_s	5.76	0.07	0.08	0.15
Se_6	D_{3d}	1.48			
Se_7	C_s (a)	3.32			
Se_8	D_{4d}	3.36			
Se_9	C_2	3.24			
Se_{10}	D_2	4.08			
Se_{11}	C_2 (a)	4.08			
Se_{12}	D_{3d}	3.85			

Calculations were carried out at the B3LYP/cc-pVDZ level on the geometry optimized at the same level

In many cases the above orders are rather different from those found for the $\langle\alpha^e\rangle$ values. Specifically, whereas the isomers for the Se_6, Se_7 and Se_8 clusters show $\langle\alpha^e\rangle$ data very close to each other, they exhibit different $\Delta\alpha^e$ values. Interestingly, the isoenergetic D_2 and D_{5d} Se_{10} isomers could be discriminated on the basis of their $\Delta\alpha^e$ values, which differ by ca. 70 a.u. (50 %). As for $\langle\alpha^e\rangle$, we also compare the $\Delta\alpha^e$ values of the ring-like and open forms of Se_3 and Se_4 clusters. The B3LYP/aug-cc-pVDZ//B3LYP/cc-pVDZ $\Delta\alpha^e$ values for the open Se_3 (C_{2v} symmetry) and

Se_4 (C_{2v} symmetry) clusters are calculated to be 95.22 and 91.96 a.u., respectively, increasing the $\Delta\alpha^e$ value of the corresponding cyclic cluster by a factor of 3.5 and 2.3, respectively. These findings agree with those previously obtained for the open and closed forms of O_3 [100], SO_2 [105], S_3 [81] and S_4 [81].

In the present work we also determined the dynamic electronic polarizabilities, since experimental data are nearly always observed at incident optical fields. We calculated dynamic polarizability values at the $\hbar\omega$ values of 0.04282, 0.05767 and 0.07197 a.u. These $\hbar\omega$ values are rather far from the experimental lowest-energy absorptions at ca. 0.14 a.u. for the Se_8 and Se_{12} clusters incorporated in zeolite A [23, 29]. The $\langle\alpha^e\rangle(-\omega;\omega)$ values are given in Table 6 together with the static figures for comparison. The dispersion effects here evaluated at the B3LYP/aug-cc-pVDZ level increase the static $\langle\alpha^e\rangle(0;0)$ values by 2–3, 3–6 and 5–14 %, respectively at the $\hbar\omega$ values of 0.04282, 0.05767 and 0.072 a.u. In all the cases, the largest dispersion effects are found for the Se_{11} cluster.

For the most stable Se_n isomers we determined the vibrational contributions to the polarizabilities (α^{pv} and α^{ZPVA}) at the B3LYP/cc-pVDZ level on the geometries computed at the same level. We used the smallest cc-pVDZ basis set since, differently to the electronic polarizabilities, the vibrational counterparts are little affected by basis set enlargement [81, 92, 106]. The results are reported in Table 7. In comparison to the electronic polarizabilities, the pure vibrational and ZPVA contributions are of small or modest entity. The largest effects are found for the Se_5 cluster, characterized by an $\langle\alpha^{pv}\rangle$ value which is two orders of magnitude larger than the ZPVA counterpart.

4 Conclusions

In summary, we have reported a comprehensive study of the geometries, energetics and electronic and vibrational polarizabilities of neutral Se_2 and cyclic Se_n ($n = 3$–12) clusters using conventional ab initio and DFT methods. For each cluster size, we considered a number of different structural isomers, identifying the lowest-energy cluster. The stability of the investigated clusters has been analyzed on the basis of the structural parameters, binding energy per atom, second-order difference of total energy, and the VIE–VEA gap. Our theoretically values for geometries, binding energy per atom and VIE are in reasonable agreement with the available experimental data. Even–odd oscillation behaviour is observed in the size dependence of the average Se–Se bond length, binding energy per atom, second-order difference of total energy, VIE, VEA and VIE–VEA gap. Our results indicate that the even-numbered Se_6 and Se_8 clusters are relatively more stable in comparison to their neighbour odd-numbered clusters, in agreement with experimental observations and previous theoretical studies.

A systematic investigation has been carried out to analyze the performance of different levels and basis sets to predict energetics and electronic polarizabilities. DFT polarizabilities are close to those obtained using MP2 and coupled-cluster calculations. The electron correlation effects are substantial for the binding energy, while are less significant for the second-order difference of total energy and electronic polarizabilities. On passing from the cc-pVDZ to the aug-cc-pVDZ basis set the electronic polarizabilities increase remarkably (up to 50 %), while further augmentation of the basis set is little important. The relativistic effects on the geometries and electronic polarizabilities are negligible. Both the pure vibrational and ZPVA contributions to the polarizabilities are a fraction of the electronic counterpart. The electronic dynamic polarizabilities have been calculated at the experimental laser wavelengths of 1,064, 790 and 633 nm, enhancing the static values by 2–14 %.

At the DFT-B3LYP/aug-cc-pVDZ level, the binding energy per atom for the selenium clusters is smaller than that for the sulphur clusters, the value in the limit for $n \to \infty$ decreasing by 0.44 eV (−16 %). Differently, when going from the S_n to the corresponding Se_n cluster the mean dipole polarizability per atom steadily increases, the variation for $n \to \infty$ being predicted to be 11.4 a.u. (+44 %). Open clusters are predicted to be more polarisable than closed forms. For all the investigated selenium clusters, the electronic mean dipole polarizability per atom is larger than $\langle\alpha^e\rangle$ (Se) owing to the enhanced polarizability contribution from the lone-pair densities.

References

1. Kumar V, Esfarjani K, Kawazoe Y (2002) Clusters and nanomaterials. Springer, Berlin
2. Alonso JA (2006) Structure and properties of atomic nanoclusters. Imperial College Press, London
3. Yoon B, Häkkinen H, Landman U, Wörz AS, Antonietti J-M, Abbet S, Judai K, Heiz U (2005) Science 307:403–407
4. Nagaya K, Hayakawa T, Yao M, Endo H (1996) J Non-Cryst Solids 205–207:807–810, and references therein
5. Licht S (1995) Sol Energy Mater Sol Cells 38:305–319
6. Barren AR (1995) Adv Mater Opt Electron 5:245–258
7. Tsuchiya K, Sakata M, Funyu A, Ikoma H (1995) Jpn J Appl Phys 34:5926–5932
8. Zakery A, Elliot SR (2003) J Non-Cryst Solids 330:1–12
9. Ogorelec Z, Tonejc A (2000) Mater Lett 42:81–85
10. Terasaki O, Yamakazi K, Thomas JM, Oshuna T, Watanabe D, Sanders JV, Barry JC (1987) Nature 330:58–60
11. Parise JB, MacDougall JE, Herron N, Farlee R, Sleight AW, Wang Y, Bein T, Moller T, Moroney LM (1988) Inorg Chem 27:221–228

12. Wirnsberger G, Fritzer HP, Zink R, Popitsch A, Pillep P, Behrens P (1999) J Phys Chem B 103:5797–5801
13. Poborchii VV (1998) Solid State Comm 107:513–518, and references therein
14. Goutfer-Wurmser F, Herold C, Mareche C-F, Lagrange P (1998) Mol Cryst Liq Cryst 310:51–56
15. Grigorian L, Fang S, Sumanasekera G, Rao AM, Schrader L, Eklund PC (1997) Synth Met 87:211–217
16. Donohue J (1974) The structures of the elements. Wiley, New York, p 370
17. Steudel R, Strauss E-M (1984) Adv Inorg Chem Radiochem 28:135–166
18. Cherin P, Unger P (1972) Acta Crystallogr B 28:313–317
19. Nagata K, Ishibashi K, Miyamoto Y (1981) Jpn J Appl Phys 20:463–469
20. Lucovsky G, Mooradian A, Taylor W, Wright GB, Keezer RC (1967) Solid State Comm 5:113–117
21. Cernosek Z, Holubova J, Cernoskova E (2011) J Therm Anal Calorim 103:429–433
22. Eysel HH, Sunder S (1979) Inorg Chem 18:2626–2627
23. Lin Z, Wang Z, Chen W, Lir L, Li G, Liu Z, Han H, Wang Z (1996) Solid State Comm 100:841–843
24. Goldbach A, Iton LE, Saboungi M-L (1997) Chem Phys Lett 281:69–73
25. Goldbach A, Grimsditch M, Iton L, Saboungi M-L (1997) J Phys Chem B 101:330–334
26. Goldbach A, Saboungi M-L (2003) Eur Phys J E 12:185–190
27. Li IL, Zhai JP, Launois P, Ruan SC, Tang ZK (2005) J Am Chem Soc 127:16111–16119
28. Li IL, Ruan SC, Li ZM, Zhai JP, Tang ZK (2005) Appl Phys Lett 87:071902/1–071902/3
29. Poborchii VV, Ivanova MS, Petranovskii VP, Barnakov YA, Kasuya A, Nishina Y (1996) Mater Sci Eng A 217–218:129–134
30. Poborchii VV (1996) Chem Phys Lett 251:230–234
31. Poborchii VV, Kolobov AV, Oyanagi H, Romanov SG, Tanaka K (1997) Chem Phys Lett 280:10–16
32. Poborchii VV, Kolobov AV, Caro J, Zhuravlev VV, Tanaka K (1997) Chem Phys Lett 280:17–23
33. Poborchii V, Kolobov A, Oyanagi H, Romanov S, Tanaka K (1998) Nanostruct Mat 10:427–436
34. Poborchii VV (2001) J Chem Phys 115:2707–2717
35. Poborchii VV, Satob M, Shchukarev AV (1997) Solid State Comm 103:649–654
36. Kohara S, Goldbach A, Koura N, Saboungi M-L, Curtiss LA (1998) Chem Phys Lett 287:282–288
37. Komulainen J, Laitinen RS, Suontamo RJ (2002) Can J Chem 80:1435–1443
38. Demkov AA, Sankey OF (2001) J Phys Condens Matter 13:10433–10457
39. Hohl D, Jones RO, Car R, Parrinello M (1987) Chem Phys Lett 139:540–545
40. Wrackmeyer B (2005) Struct Chem 16:67–71
41. Mikko Rautiainen J, Way T, Schatte G, Passmore J, Laitinen RS, Suontamo RJ, Valkonen J (2005) Inorg Chem 44:1904–1913
42. Orlova G, Goddard JD (1999) J Phys Chem A 103:6825–6834
43. Goddard JD, Chen X, Orlova G (1999) J Phys Chem A 103:4078–4084
44. Li ZQ, Yu JZ, Ohno K, Gu BL, Czajka R, Kasuya A, Nishina Y, Kawazoe Y (1995) Phys Rev B 52:1524–1527
45. Heinemann C, Koch W, Lindner G-G, Reinen D, Widmark P-O (1996) Phys Rev A 54:1979–1993
46. Beck DR, Key RJ, Slaughter AR, Mathews RD, Banna MS (1983) Phys Rev A 28:2634–2640
47. Oligschleger C, Jones RO, Reimann SM, Schober HR (1996) Phys Rev B 53:6165–6173
48. Pan BC, Han JG, Yang J, Yang S (2000) Phys Rev B 62:17026–17030
49. Xu W, Bai W (2008) J Mol Struct (Theochem) 854:89–105
50. Lippincott ER, Nagarajan G, Stutman JM (1966) J Phys Chem 70:78–84
51. Torrent-Sucarrat M, De Proft F, Geerlings P (2005) J Phys Chem A 109:6071–6076
52. Lee C, Yang W, Parr RG (1988) Phys Rev B 37:785–789
53. Becke AD (1993) J Chem Phys 98:5648–5652
54. Woon DE, Dunning TH (1994) J Chem Phys 100:2975–2988
55. Sekino H, Bartlett RJ (1986) J Chem Phys 85:976–989
56. Karna SP, Dupuis M (1991) J Comput Chem 12:487–504
57. Kurtz HA, Stewart JJP, Dieter KM (1990) J Comput Chem 11:82–87
58. Yanai T, Tew D, Handy NC (2004) Chem Phys Lett 393:51–57
59. Champagne B, Perpète EA, van Gisbergen SJA, Baerends E-J, Snijders JG, Soubra-Ghaoui C, Robins KA, Kirtman B (1998) J Chem Phys 109:10489–10498
60. Jacquemin D, Perpète EA, Scalmani G, Frisch MJ, Kobayashi R, Adamo C (2007) J Chem Phys 126:144105/1–144105/12
61. Limacher PA, Mikkelsen KV, Luthi HP (2009) J Chem Phys 130:194114/1–194114/7
62. Alparone A (2011) Chem Phys Lett 514:21–25
63. Maroulis G (2011) Theor Chem Acc 129:437–445
64. Feller D (1996) J Comput Chem 17:1571–1586
65. Schuchardt KL, Didier BT, Elsethagen T, Sun L, Gurumoorthi V, Chase J, Li J, Windus TL (2007) J Chem Inf Model 47:1045–1052
66. Sadlej AJ (1991) Theoret Chim Acta 81:45–63
67. Rice JE, Handy NC (1991) J Chem Phys 94:4959–4971
68. Douglas M, Kroll NM (1974) Ann Phys 82:89–155
69. Hess BA (1986) Phys Rev A 33:3742–3748
70. Jansen G, Hess BA (1989) Phys Rev A 39:6016–6017
71. Benkova Z, Sadlej AJ (2004) Mol Phys 102:687–699. Available from: http://www.qch.fns.uniba.sk/Baslib/POL_DK
72. Wilson AK, Woon DE, Peterson KA, Dunning TH Jr (1999) J Chem Phys 110:7667–7676
73. Bishop DM (1998) Adv Chem Phys 104:1–40
74. Kirtman B, Champagne B (1997) Int Rev Phys Chem 16:389–420
75. Luis L, Duran M, Champagne B, Kirtman B (2000) J Chem Phys 122:5203–5213
76. Champagne B, Luis JM, Duran M, Andrés JL, Kirtman B (2000) J Chem Phys 112:1011–1020
77. Bishop DM, Sauer SPA (1997) J Chem Phys 107:8502–8509
78. Perpète EA, Champagne B, Kirtman B (1997) J Chem Phys 107:2463–2480
79. Frisch MJ, Trucks GW, Schlegel HB, Scuseria GE, Robb MA, Cheeseman JR, Scalmani G, Barone V, Mennucci B, Petersson GA, Nakatsuji H, Caricato M, Li X, Hratchian HP, Izmaylov AF, Bloino J, Zheng G, Sonnenberg JL, Hada M, Ehara M, Toyota K, Fukuda R, Hasegawa J, Ishida M, Nakajima T, Honda Y, Kitao O, Nakai H, Vreven T, Montgomery JA Jr, Peralta JE, Ogliaro F, Bearpark M, Heyd JJ, Brothers E, Kudin KN, Staroverov VN, Kobayashi R, Normand J, Raghavachari K, Rendell A, Burant JC, Iyengar SS, Tomasi J, Cossi M, Rega N, Millam JM, Klene M, Knox JE, Cross JB, Bakken V, Adamo C, Jaramillo J, Gomperts R, Stratmann RE, Yazyev O, Austin AJ, Cammi R, Pomelli C, Ochterski JW, Martin RL, Morokuma K, Zakrzewski VG, Voth GA, Salvador P, Dannenberg JJ, Dapprich S, Daniels AD, Farkas O, Foresman JB, Ortiz JV, Cioslowski J, Fox DJ (2009) Gaussian 09 revision A. 02. Gaussian, Wallingford
80. Alparone A (2012) Comput Theor Chem 988:81–85
81. Millefiori S, Alparone A (2001) J Phys Chem A 105:9489–9497

82. Mills KC (1974) Thermodynamic data for inorganic sulphides, selenides and tellurides. Butterworths, London
83. Kirtman B (1988) Chem Phys Lett 143:81–83
84. Toto JL, Toto TT, de Melo CP, Robins KA (1995) J Chem Phys 102:8048–8052
85. Hoareau A, Reymond JM, Cabaud B, Uzan R (1975) J Phys (Paris) 36:737–743
86. Becker J, Rademann K, Hensel F (1991) Z Phys D 19:233–235
87. Tribottet B, Benamar A, Rayane D, Melinon P, Broyer M (1993) Z Phys D 26:352–354
88. Igel-Mann G, Stoll H, Preuss H (1993) Mol Phys 80:341–354
89. Snodgrass JT, Coe JV, McHugh KM, Freidhoff CB, Bowen KH (1989) J Phys Chem 93:1249–1254
90. Bonin KD, Kresin VV (1997) Electric-dipole polarizabilities of atoms, molecules and clusters. World Scientific, Singapore
91. Millefiori S, Alparone A (1998) J Mol Struct (Theochem) 422:179–190
92. Millefiori S, Alparone A (2004) Chem Phys 303:27–36
93. Hurst GB, Dupuis M, Clementi E (1988) J Chem Phys 89:385–395
94. Kirtman B, Hasan M (1992) J Chem Phys 96:470–479
95. Hohm U, Goebel D, Karamanis P, Maroulis G (1998) J Phys Chem A 102:1237–1240
96. Maroulis G, Xenides D (2003) J Phys Chem A 107:712–719
97. Miller TM, Bederson B (1977) Adv Atom Mol Phys 13:1–55
98. Chattaraj PK, Segupta S (1996) J Phys Chem 100:16126–16130
99. Ghanty TK, Ghosh SK (1996) J Phys Chem 100:12295–12298
100. Maroulis G (1999) J Chem Phys 111:6846–6849
101. Maroulis G, Begué D, Pouchan C (2003) J Chem Phys 119:794–797
102. Maroulis G, Pouchan C (2003) Phys Chem Chem Phys 5:1992–1995
103. Gough KM (1989) J Chem Phys 91:2424–2432
104. Laidig KE, Bader RFW (1990) J Chem Phys 93:7213–7224
105. Xenides D, Maroulis G (2001) J Chem Phys 115:7953–7956
106. Millefiori S, Alparone A (2000) Phys Chem Chem Phys 2:2495–2501